Pressure-induced metallization, transition to the pyrite-type structure, and superconductivity in palladium disulfide PdS_2

M. A. ElGhazali,[1,2] P. G. Naumov,[1,3] Q. Mu,[1] V. Süß,[1] A. O. Baskakov,[3] C. Felser,[1] and S. A. Medvedev[1]

[1]*Max Planck Institute for Chemical Physics of Solids, Dresden 01187, Germany*

[2]*Institute for Solid State Physics, Technical University Dresden, Dresden 01069, Germany*

[3]*Shubnikov Institute of Crystallography of Federal Scientific Research Centre "Crystallography and Photonics" of Russian Academy of Sciences, Moscow 119333, Russia*

(Received 10 May 2019; revised manuscript received 25 June 2019; published 11 July 2019)

The pressure effect on crystal structures, lattice vibrations, and electrical transport properties of PdS_2 and $NiSe_2$ were studied under high pressures of up to ∼50 GPa using Raman spectroscopy and electrical resistivity measurements. PdS_2 undergoes semiconductor-to-metal transition at a pressure of ∼7 GPa without a structural phase transition. Structural transition to the pyrite-type phase occurs at a pressure of ∼16 GPa. Superconductivity emerges in the pyrite-type phase of PdS_2 with a well-defined dome-shaped dependence of critical temperature of superconductivity on pressure, with a maximum value of 8.0 K at 37.4 GPa. Although this behavior is similar to that in isostructural $PdSe_2$, correlation with anomalous anion bond softening at critical temperature is not observed in PdS_2 in contrast to $PdSe_2$. Conversely, the anion bond instability is observed by the softening of the Se_2^{2-} internal vibrational Raman mode in pyrite $NiSe_2$ under pressure. Despite the persisting structural instability due to destabilization of Se_2^{2-} dimers, $NiSe_2$ remains a normal nonsuperconducting metal.

DOI: 10.1103/PhysRevB.100.014507

I. INTRODUCTION

Superconductivity with relatively high critical temperature (T_c) often emerges in compounds with structural instabilities associated with phonon softening, resulting in strongly enhanced electron-phonon coupling. A class of compounds much discussed in this respect are the A15 superconductors with general chemical formula A_3B (A = group IVb−VIb element, B = group IIIa−Va element) of which some are close to structural distortions [1,2]. The systematic tuning of chemical bonds as a structural parameter (by applied physical or chemical pressure) driving the system toward structural instability was demonstrated to be useful to control physical properties [3] and to enhance or even induce the superconductivity [4–7].

Transition metal dichalcogenides TX_2 (where T denotes the transition metal and X refers to the chalcogenide atom) with a pyrite structure containing quasimolecular X_2^{2-} dimers are an excellent system to analyze bonding systematics because electronic effects in these compounds are correlated with nonmetal-nonmetal bond strength [8–10]. Superconductivity in pyrite superconductors [11–14] might correlate with structural instability caused by destabilization of anion dimers. Superconductivity with the highest critical temperature emerges in these compounds in the vicinity of the weakest Se_2^{2-} bonds tuned by chemical substitution in defective pyrite $Ir_{0.94-x}Rh_xSe_2$ (9.6 K for $x = 0.36$) [11], or by pressure in the high-pressure pyrite phase of $PdSe_2$ (13.1 K at 23 GPa) [14]. To obtain further insight into the interplay between superconductivity and the bond strength of anion dimers in the pyrite structure, we performed experimental studies of lattice dynamics and electrical resistivity of PdS_2 (isostructural with $PdSe_2$ at ambient conditions) and pyrite $NiSe_2$ under high pressure.

II. EXPERIMENTAL DETAILS

Single crystal samples of PdS_2 and $NiSe_2$ for this study were grown using the chemical vapor transport method. The compounds PdS_2 and $NiSe_2$ have first been synthesized by a direct reaction of the elements Pd (Alfa Aesar 99.95%) and S (Alfa Aesar 99.999%) at 550 °C and Ni (Alfa Aesar 99.996%) and Se (Alfa Aesar 99.999%) at 800 °C in evacuated fused silica tubes over 10 days. Phase purity of the obtained microcrystalline powder was proven by x-ray powder diffraction. Starting from the microcrystalline powder, single crystals of PdS_2 and $NiSe_2$ have been grown by a chemical transport reaction in a temperature gradient from 600 °C (source) to 500 °C (sink) with $PdCl_2$ (Alfa Aesar 99.9%) as the transport additive and in a temperature gradient from 800 °C (source) to 700 °C (sink) using $SeCl_4$ as the transport additive, respectively. The stoichiometry of the obtained crystals was proven using energy dispersive x-ray spectroscopy to be close to a nominal composition (33.2 at. % of Pd and 66.8 at. % of S for PdS_2 and 32.9 at. % of Ni and 67.1 at. % of Se for $NiSe_2$) uniformly across the sample. The Raman spectra of the samples collected at ambient pressure are in good agreement with literature data proving the crystal structure of obtained single crystals.

A screw-clamped diamond anvil cell equipped with 500-μm culet diamond anvils was used for the simultaneous Raman spectroscopy and electrical resistivity measurements. The gasket was made of a 300-μm thick tungsten foil. For electrical resistivity measurements, the tungsten gasket was insulated with a cubic BN/epoxy mixture. Single crystal samples of a near-square shape ∼120-μm size and ∼5–10-μm thickness were loaded in the sample chamber (diameter 200 μm and height 40 μm) filled with NaCl as the pressure-

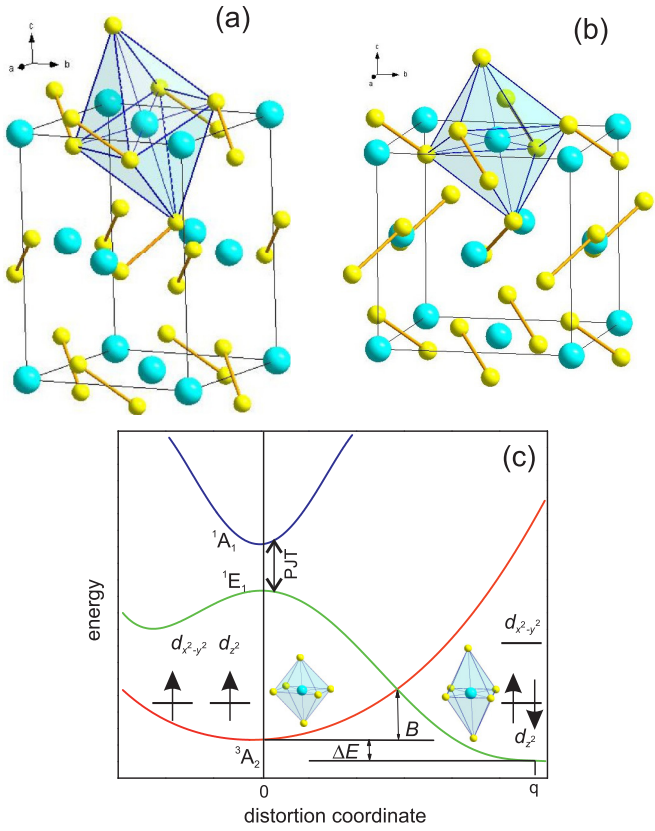

FIG. 1. The ambient-pressure crystal structure of PdS_2 (a) is a distorted pyrite structure (b). (c) Schematic dependence of the energy of the electronic states of the half-filled e^2 system on deformation coordinate q (E mode). Strong vibrational coupling between excited states (hidden pseudo-Jahn-Teller effect, PJT) makes the distorted configuration with the doubly occupied d_{z^2} orbital energetically favorable (energy separation ΔE and energy barrier B). (Adapted from Ref. [16]).

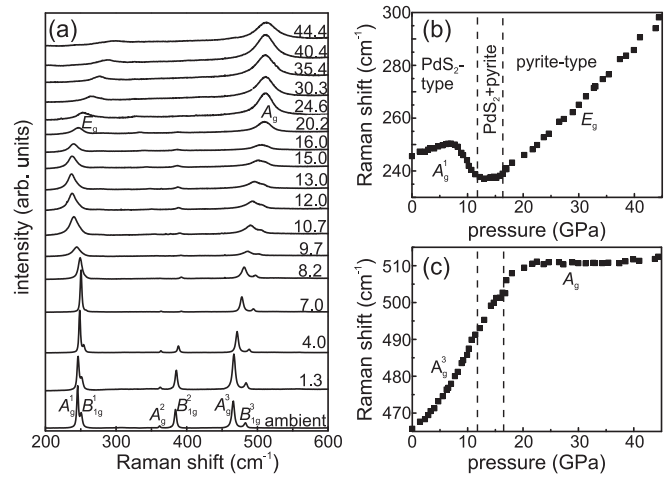

FIG. 2. (a) Selected Raman spectra of PdS_2 collected at a pressure increase run. Numbers denote pressure values in GPa. Mode assignment for the PdS_2-type structure is presented at the ambient pressure spectrum, and for the pyrite-type structure, at 20.2 GPa. (b) and (c) Pressure dependence of the frequencies of the librational $A_g{}^1$ mode (double degenerated E_g mode in the pyrite phase) and the $A_g{}^3$ symmetric stretching mode (A_g mode in the pyrite phase) of the $S_2{}^{2-}$ anions, respectively. Dashed lines indicate tentative phase boundaries drawn by analogy with $PdSe_2$ (Appendix).

transmitting medium. Four electrical leads fabricated from 5-μm-thick Pt foil were contacted by application of pressure to the surface of the sample in the van der Pauw configuration. Electrical resistivity was measured with a direct current, in temperature range from 1.4 K to room temperature.

Raman spectra were collected at room temperature in backscattering geometry using a customary confocal micro-Raman spectrometer equipped with 20 × long working distance objective, HeNe laser as the excitation source, and a single-grating spectrograph with 1 cm^{-1} resolution. Pressure was measured *in situ* with an accuracy of ∼0.1 GPa using the standard ruby fluorescence scale.

III. RESULTS AND DISCUSSION

A. Suppression of structural distortion, metallization, and transition to the pyrite-type structure

PdS_2 and $PdSe_2$ at normal pressure crystalize into the unique orthorhombic PdS_2-type structure belonging to the *Pbca* space group [Fig. 1(a)], which is a distorted pyrite structure [Fig. 1(b)] with the PdS_6 octahedra elongated along the c axis, leading to a square-planar coordination of Pd. This distortion resembles the cooperative Jahn-Teller (JT) effect [15]. However, in the symmetrical octahedral coordination, the lowest state according to Hund's rule is the spin-triplet $^3A_2$ state of the Pd (d^8) cation. This is an orbitally nondegenerated state and thus not of JT nature. Because the lowest exited states ^1E and $^1A_1$ have spin multiplicity different from that of the ground $^3A_2$ state, there is also no pseudo (second-order) JT effect for the ground state. If the excited $^1A_1$ and ^1E states are close in energy with sufficiently strong JT-like vibrational coupling between them [hidden pseudo-JT effect (PJT)] [16], the energy gap to the ground term might be overcome, and the distorted configuration with singlet electronic state becomes energetically favorable [Fig. 1(c)]. Such a situation is apparently realized in PdS_2 and $PdSe_2$ (as the only source of instability and distortion of the high-symmetry system configuration in the nondegenerate state [16,17]) due to strong coupling between the half-filled electronic shell system e^2 and the E_g lattice mode in the undistorted pyrite-type structure with symmetric octahedral coordination. This leads to the structural distortion, with electrons filling the lower d_{z^2} orbitals [Fig. 1(c)]. This configuration accounts for the diamagnetic semiconducting properties of PdS_2 ($PdSe_2$) at ambient pressure conditions.

Application of external pressure eliminates the structural distortion of $PdSe_2$, rendering the pyrite-type structure stable at pressures above 11 GPa, as established by high-pressure structural [15] and Raman spectroscopy [14] studies. According to the pressure homology principle, the same structural transition can also be expected in PdS_2 at higher pressures. Indeed, pressure evolution of the Raman spectra of PdS_2 [Fig. 2(a)] indicates high-pressure transformation to the pyrite-type structure in PdS_2.

The Raman spectrum of PdS_2 at the ambient pressure [Fig. 2(a)] is similar to that of bulk isostructural $PdSe_2$ [18], with all peaks shifted to higher frequencies due to the lighter

atomic mass of the sulfur atoms. Thus, the mode assignment of all peaks can be conducted in the same manner as for $PdSe_2$ [18]. From 12 Raman active modes following from the group analysis ($3A_g + 3B_{1g} + 3B_{2g} + 3B_{3g}$), only three A_g and three B_{1g} modes have been observed in unpolarized Raman measurements similarly to the experimental observation in related compound $PdSe_2$ [18], for which theoretical calculations revealed that only these modes have nonzero Raman tensor elements [18]. The atomic vibrations observed in the Raman spectra involve only chalcogen atoms. The A_g^1 and A_g^3 modes correspond to the librational and internal stretching vibrational motions of the S dumbbells respectively, whereas the other modes are combinations of these vibrations.

Application of pressure leads to the gradual merging of A_g^1 with B_{1g}^1 and A_g^3 with B_{1g}^3 peaks in course of the suppression of structural distortion and the concomitant gradual redistribution of the peak intensities in Raman spectra [Fig. 2(a)]. The high-pressure spectra are dominated by two peaks, which might be assigned to the doubly degenerated E_g librational and A_g symmetric internal vibrational stretching of the S_2^{2-} dimers modes in the cubic pyrite-type structure (the less intense T_g modes expected in the pyrite structure might be screened by broadened E_g and A_g peaks) owing to the similarity to the high-pressure Raman spectra of $PdSe_2$ [14]. However, the continuous gradual changes in the spectra make it difficult to determine the pressure of the structural transition. Analysis of the peculiar pressure dependence of the frequency of the librational A_g^1 mode [Fig. 2(b)] allows one to determine the pressure of the structural phase transition to the pyrite-type phase.

The frequency of the librational A_g^1 mode initially increases up to a pressure of 7 GPa (at the rate of $\sim 0.7\,cm^{-1}$/GPa), demonstrating normal behavior upon compression. The mode frequency starts to decrease rapidly upon further pressure increases of up to ~12 GPa, and becomes nearly pressure-independent in the pressure range of 12–16 GPa. Above 16 GPa, the frequency starts monotonously increasing again up to the highest applied pressure in this experiment. Such peculiar dependence of the frequency on pressure in PdS_2 is qualitatively similar to that observed for the same lattice mode in $PdSe_2$ (see the Appendix). Thus, by analogy with $PdSe_2$, the pressure of 16 GPa, at which the librational frequency starts increasing again, delimits the accomplishment of the structural transition to the pyrite-type phase in PdS_2, whereas both PdS_2-type and pyrite-type phases coexist in the pressure range of 12–16 GPa.

The softening of the librational A_g^1 mode frequency above 7 GPa indicates an increase in the intralayer Pd-S distances, similar to what has been established for the intralayer Pd-Se distances in $PdSe_2$ [15] (see the Appendix). Such atomic displacement corresponds to the filling of the $d_{x^2-y^2}$ orbitals of the Pd atoms [19]. Indeed, the interlayer cation-anion distances decrease sharply upon compression [15], leading to strong enhancement in the overlap repulsion between the filled d_{z^2} orbitals of the Pd cation and the π^* shell of the S_2^{2-} anion from the adjacent layer. This enhanced repulsion modifies the energy landscape [Fig. 1(c)], decreasing the energy difference ΔE and barrier height B and enabling the tunneling between the singlet and triplet electronic terms. Thus, both distorted

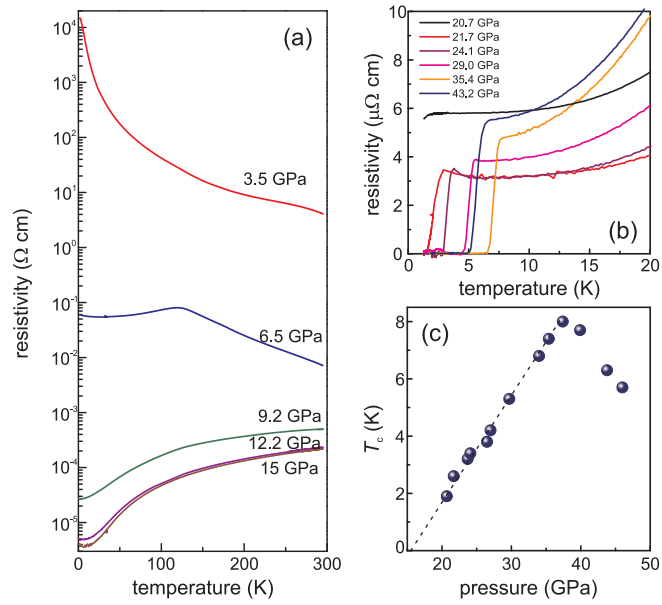

FIG. 3. (a) Application of pressure tunes the electronic properties of PdS_2 from a semiconductor to a metal at pressures above 7 GPa. (b) In the high-pressure pyrite phase of PdS_2, superconductivity emerges with T_c showing a dome-shaped dependence on pressure (c) with the maximum T_c of 8.0 K at a pressure of ~37.4 GPa.

(with the doubly occupied d_{z^2} orbital) and undistorted (with the electrons distributed between the d_{z^2} and $d_{x^2-y^2}$ orbitals) configurations coexist dynamically in this situation. This leads to a change in the electronic transport properties of PdS_2: Semiconducting at low pressures, PdS_2 shows metallic behavior in the whole temperature range of 1.4–300 K at pressures above 7 GPa [Fig. 3(a)]. PdS_2 remains a normal metal (with no superconductivity down to 1.4 K) up to the structural transition to the pyrite-type phase at 16 GPa [Fig. 3(a)].

Such behavior is similar to that of $PdSe_2$ (see the Appendix) undergoing semiconductor-to-metal transition at 3 GPa within the PdS_2-type structure [14] concomitantly with the onset of the softening of the A_g^1 mode (Appendix). However, in contrast to $PdSe_2$ showing a softening of the internal stretching A_g^3 mode of the Se dimers (elongation of Se−Se bonds) at pressures above 3 GPa (Appendix), only a monotonic hardening of the stretching mode, without any anomalies due to S−S dimer elongation, is revealed in PdS_2 up to the transition in the pyrite-type structure [Fig. 2(c)]. Thus, the metallization in PdX_2 (X = S, Se) is driven by the population of the $d_{x^2-y^2}$ orbitals of Pd (which are strongly hybridized with chalcogen p orbitals, forming the conduction band [14]), caused by the suppression of the structural distortion (hidden PJT effect). This might be considered as evidence of orbital selective metallization: While electrons in the d_{z^2} orbitals remain localized due to persisting structural distortion, the filling of the $d_{x^2-y^2}$ orbitals drives the semiconductor-to-metal transition.

B. Superconductivity in the high-pressure pyrite-type phase of PdS_2

Similar to $PdSe_2$ [14], PdS_2 in the high-pressure pyrite-type structure becomes superconducting at low temperatures

[Fig. 3(b)]. The resistivity curve at ~20.7 GPa shows a drop in the resistivity at temperature below ~2 K [Fig. 3(b)], suggesting the onset of a superconducting transition. The superconducting state is clearly observed at higher pressures, with the resistivity dropping abruptly to zero.

The critical temperature of superconductivity (T_c) demonstrates a well-defined dome-shaped dependence on pressure. Initially, T_c increases as the pressure increases [Fig. 3(c)] at a rate of ~0.35 K/GPa (noticeably, this rate is considerably lower than ~1.2 K/GPa observed in the sister compound $PdSe_2$ [14]). The increase of the T_c with pressure in PdS_2 falls within the wide range of dependences observed in transition metals superconductors where a positive sign of dT_c/dP arises from a rapid increase of the Hopfield parameter $\eta = N(E_f)\langle I^2\rangle$ [where $N(E_f)$ is the electronic density of states at the Fermi energy and $\langle I^2\rangle$ is the average electronic matrix element] [20]. The maximum T_c value of 8.0 K is reached at a pressure of 37.4 GPa. Above this pressure and up to the highest experimental pressure of 46 GPa, T_c decreases continuously. The dome-shaped dependence of T_c is conditioned apparently by the completion of the pressure-induced increase of the Hopfield parameter (reflecting the character of the electrons near Fermi energy) and the stiffening of the lattice vibration spectrum. The later effect dominates apparently at high pressure leading to decrease of T_c at high pressures. Theoretical calculations of the electronic structure and electron-phonon coupling in dependence on pressure are necessary to understand the dome-shaped dependence of T_c on pressure.

Thus, the electronic transport properties of PdS_2 in the high-pressure pyrite-type phase are qualitatively similar to those of $PdSe_2$ [14]. However, in contrast to $PdSe_2$ which shows an obvious correlation between pressure dependences of T_c and the bonding strength of Se–Se dumbbells [14], the anions' internal vibration frequency in the pyrite-phase of PdS_2 is nearly independent of pressure, without any anomalies due to the softening of the S–S bonding [Fig. 2(c)]. This behavior of the frequency of the internal vibration of the S_2^{2-} anions in PdS_2 is similar to the dependence of the A_g mode frequency on pressure in pyrite NiS_2 [9]. Thus, the destabilization of the chalcogen dumbbells is not the necessary parameter leading to the emergence of superconductivity in the pyrite compounds. However, T_c for pyrite superconductors $PdSe_2$ and $Ir_{0.94-x}Rh_xSe_2$ shows striking correlations with the bond strength of the Se_2^{2-} anions [11,14]. The bond softening is a result of charge transfer from the cation to Se_2^{2-} dimers [10] leading to changes in the electronic system (effective "hole self-doping") and thus influencing the T_c value and provoking the correlation between T_c and the bond strength of the anions.

C. Nonsuperconducting pyrite $NiSe_2$ under high pressure

NiS_2 and $NiSe_2$, which are isoelectronic with PdS_2 and $PdSe_2$, crystalize at ambient pressure in the undistorted pyrite structure, with octahedral coordination of the Ni cations in the high spin state. It is proposed that strong on-site repulsion U in the doubly occupied d_{z^2} orbitals of Ni prevents the structural distortion to the PdS_2-type structure in the Ni dichalcogenides [15]. NiS_2 is a typical strongly correlated antiferromagnetic insulator undergoing the insulator-to-metal transition under application of pressures of ~2.5–3 GPa or by Se substitution in $NiS_{2-x}Se_x$ at $x \sim 0.6$ by preserving the cubic pyrite-type structure [21]. $NiSe_2$ is a normal metal at ambient conditions [22]. Remarkably, theoretical calculations revealed the anomalous behavior (elongation) of the Se–Se bond length in $NiSe_2$ under compression [8]. It is interesting to prove this finding experimentally and to check if this bonding instability leads to the pressure-induced superconductivity in $NiSe_2$.

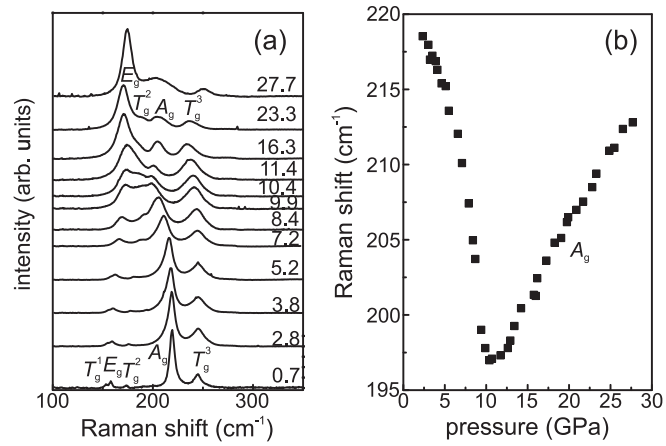

FIG. 4. (a) Selected Raman spectra of $NiSe_2$ collected at a pressure increase run. Numbers denote pressure values in GPa. Mode assignment for the pyrite-type structure is presented for spectra at 0.7 and 23.3 GPa. (b) Pressure dependence of the frequency of the symmetrical stretching A_g mode of the Se_2^{2-} anion.

The Raman spectra of $NiSe_2$ in the diamond anvil cell at low pressures [Fig. 4(a)] are in good agreement with data from the literature [23]. All five Raman-active modes ($A_g + E_g + 3T_g$) predicted by factor group analysis for a pyrite-type structure could be identified in the spectra. Application of pressure led to shifting of the observed peaks and redistribution of intensities [Fig. 4(a)]. However, all Raman-active modes of the pyrite structure could be identified up to the highest pressures used in this study [Fig. 4(a); the low-frequency T_g^1 and E_g lines merge into a single band, as in NiS_2, under pressure [9], indicating structural stability of the pyrite-type structure of $NiSe_2$ at least up to pressures of ~30 GPa.

Interestingly, the frequency of the internal vibrations (A_g mode) of the Se dimers demonstrates anomalous softening under compression [Fig. 4(b)], which is in agreement with the theoretically predicted elongation of the Se–Se distance [8]. This elongation is caused by electron transfer from the Ni d orbitals to the antibonding σ^* states of the Se_2^{2-} dumbbells [10]. The A_g mode softening in $NiSe_2$ is qualitatively similar to the Se–Se bond softening in the high-pressure pyrite phase of $PdSe_2$ [14]. Remarkably, the intensity of the E_g mode increases relative to the intensity of the A_g mode as pressure increases [Fig. 4(a)], which, once again, shows behavior similar to that observed in the pyrite phase of $PdSe_2$ [14] with the softening of Se–Se bonds, but is in striking contrast to those in the pyrite phase of PdS_2 [Fig. 2(a)] and pyrites FeS_2 [24] and NiS_2 [9] with the rigid S_2^{2-} dumbbells.

Thus, $NiSe_2$ demonstrates Se–Se bond instability under pressure, similar to the superconducting pyrite phase of $PdSe_2$, in which the dependence of T_c on pressure shows

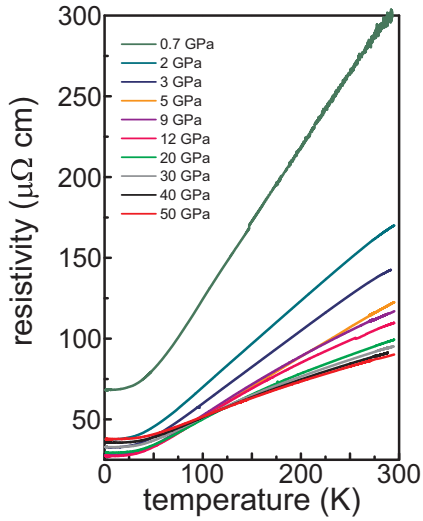

FIG. 5. Temperature dependence of the electrical resistivity of $NiSe_2$ at different pressures.

a striking correlation with the bonding strength of Se–Se dumbbells [14]. Despite this similarity in lattice dynamics, $NiSe_2$ remains a normal metal up to 50 GPa (Fig. 5), with no evidence of superconducting transition at T_c values above 1.4 K. This indicates, once again, that the structural instability due to the destabilization of the chalcogen dumbbells is not the sufficient condition governing the appearance of superconductivity in compounds with a pyrite structure.

It might be assumed that strong electron correlations in Ni prevent superconductivity in $NiSe_2$. However, because superconductivity at relatively high T_c is observed in the pyrite compounds of 4*d* and 5*d* transition metals [11–14], the spin-orbit coupling might play an important role in superconductivity in these compounds. So for $PdSe_2$, the *ab initio* electronic band structure calculations indicate the presence of Dirac and nodal-line fermions in the vicinity of the Fermi energy protected by the pyrite structure symmetry, which can lead to interesting superconducting states [14]. Because superconductivity with qualitatively similar pressure behavior is observed in PdS_2 and $PdSe_2$, independent of different anion bond behaviors, it might be suggested that proximity to the structural instability, which leads to the distortion of the pyrite structure (hidden PJT effect), is important for the emergence of superconductivity in the high-pressure pyrite-type phases of Pd dichalcogenides. This structural instability is caused by the strong coupling between the half-filled e_g electronic shell and librational E_g lattice mode in the pyrite structure. This strong coupling manifests in correlation between evolution of the electronic transport properties and anomalous pressure dependence of the librational modes in PdS_2 and $PdSe_2$. Therefore, it might be suggested that strong electron-phonon coupling between electrons populating e_g shells and librational E_g modes leads to the superconductivity in Pd compounds pyrite structure. It is suggested to be general for pyrite superconductors since the superconductivity in compounds with pyrite structure was observed only in compounds with partially filled electronic e_g orbitals, while the pyrite

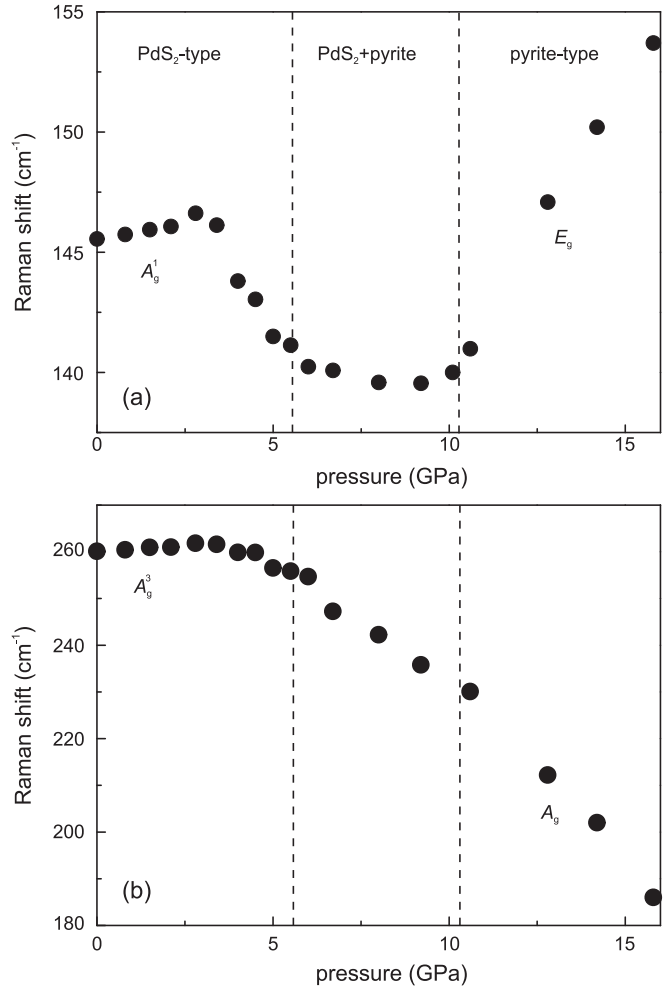

FIG. 6. Pressure dependence of the frequencies of (a) the librational $A_g{}^1$ mode (double degenerated E_g mode in the pyrite phase) and (b) $A_g{}^3$ symmetric stretching mode (A_g mode in the pyrite phase) of the $Se_2{}^{2-}$ anions in $PdSe_2$. Dashed lines indicate the phase boundaries from high-pressure structural studies of $PdSe_2$ [15].

compounds with empty e_g orbitals (like $RuSe_2$, $OsSe_2$ and $OsTe_2$) undergoing metal to insulator transition at ~20 GPa without any anomalies of the lattice vibrations, remain nonsuperconducting up to pressures beyond 50 GPa [25]. This suggestion however, needs to be proven by studies of lattice dynamic of other pyrite superconductors like $Ir_{0.94-x}Rh_xSe_2$ in dependence on x and pressure and theoretical calculations.

IV. CONCLUSIONS

Raman spectroscopy studies of PdS_2 reveal a structural phase transition from the PdS_2 type to the pyrite-type structure at a pressure of approximately 16 GPa. Application of pressure drastically changes the electronic transport properties of PdS_2. A semiconductor at ambient pressure, PdS_2 becomes a metal at pressures above 7 GPa. The metallization is concomitant with a softening of the vibrational mode due to increasing intraplane cation-anion distances, indicative of the population of the Pd $d_{x^2-y^2}$ orbitals. Superconductivity emerges in PdS_2

after the structural transition to the pyrite-type phase above 16 GPa. T_c demonstrates dome-shaped dependence on pressure, with the maximum T_c value being 8.0 K at 37.4 GPa. Thus, the pressure evolution of the electronic transport properties of PdS_2 is qualitatively similar to that of $PdSe_2$. Despite this similarity in electronic properties, correlating with T_c anomalous softening of the anion dumbbells in PdS_2 was not observed, in contrast to $PdSe_2$. On the other hand, the Se–Se bond instability was clearly observed in pyrite $NiSe_2$ under pressure while it remains a normal nonsuperconducting metal. These observations imply insufficiency of a direct correlation between structural instability due to the destabilization of chalcogen dimers and the emergence of superconductivity in the pyrite compounds. Because the electronic properties of the pyrite compounds are depending on the bond strength of the anions, the T_c in these compounds might be further tuned by tuning the nonmetal-nonmetal bond strength by application of chemical or physical pressure. However, the superconductivity in these compounds is driven most likely by other structural instabilities. The proximity to a structural distortion due to the strong electron-lattice coupling (hidden PJT effect) in PdS_2 and $PdSe_2$ might be viewed as the structural instability driving the emergence of superconductivity in the high-pressure pyrite phases of the Pd dichalcogenides.

ACKNOWLEDGMENTS

This work was supported by the DFG under Projects No. ME 3652/3-1 and No. GRK 1621. P.G.N. acknowledges the support provided by the Russian Science Foundation (Project No. 17-72-20200). The authors thank M. Schmidt for help with the sample synthesis and W. Schnelle for critical reading and suggestions for improving the manuscript.

APPENDIX: LATTICE DYNAMICS AND STRUCTURAL TRANSITION TO THE PYRITE-TYPE STRUCTURE IN $PdSe_2$

The Raman spectroscopy studies [14] indicate pressure-induced structural phase transition to the pyrite-type structure, which is in good agreement with a structural investigation of $PdSe_2$ [15]. Pressure dependence of the frequencies of the A_g^1 librational (the doubly degenerated E_g mode in the pyrite-type structure) and the A_g^3 internal stretching of the modes of the Se_2 dumbbells in the PdS_2-type structure in the pressure region of the structural phase transition are shown in Fig. 6. The frequency of the A_g^1 mode increases slightly when the pressure increases up to ~3 GPa. Above this pressure, the frequency shows significant softening up to a pressure of ~6 GPa. The frequency softening is in agreement with the increase in the intralayer Pd–Se distances observed in the structural studies [15]. Remarkably, at a pressure of ~3 GPa, at which the softening of the A_g^1 mode begins, $PdSe_2$ undergoes a semiconductor-to-metal transition [14], indicating strong charge-lattice coupling. In a pressure range of 6–11 GPa, the A_g^1 mode is nearly independent of pressure [Fig. 6(a)]. According to high-pressure structural studies, the PdS_2-type and pyrite-type phases coexist in this pressure range [15]. The A_g^1 mode frequency starts increasing continuously at pressures above 11 GPa [Fig. 6(a)] indicating the completeness of transition to the pyrite-type structure, which is also in agreement with the results of past structural studies [15]. Notably, the frequency of the internal vibrations of Se_2^{2-} dimers also demonstrates softening at pressures above 3 GPa [Fig. 6(b)]. There are no discontinuities in the pressure dependence of the frequency in this mode at the transition to the pyrite-type structure [Fig. 6(b)] and the pressure dependence of this mode frequency correlates further with the critical temperature of the superconductivity emerging in the pyrite structure [14].

[1] L. R. Testardi, Rev. Mod. Phys. **47**, 637 (1975).
[2] G. R. Stewart, Phys. C **514**, 28 (2015).
[3] S. Jia, P. Jiramongkolchai, M. R. Suchomel, B. H. Toby, J. G. Checkelsky, N. P. Ong, and R. J. Cava, Nat. Phys. **7**, 207 (2011).
[4] D. Hirai, F. von Rohr, and R. J. Cava, Phys. Rev. B **86**, 100505(R) (2012).
[5] S. Pyon, K. Kudo, and M. Nohara, J. Phys. Soc. Jpn. **81**, 053701 (2012).
[6] S. Kitagawa, H. Kotegawa, H. Tou, H. Ishii, K. Kudo, M. Nohara, and H. Harima, J. Phys. Soc. Jpn. **82**, 113704 (2013).
[7] K. Kudo, H. Ishii, and M. Nohara, Phys. Rev. B **93**, 140505(R) (2016).
[8] J. Kuneš, L. Baldassarre, B. Schächner, K. Rabia, C. A. Kuntscher, D. M. Korotin, V. I. Anisimov, J. A. McLeod, E. Z. Kurmaev, and A. Moewes, Phys. Rev. B **81**, 035122 (2010).
[9] C. Marini, A. Perucchi, D. Chermisi, P. Dore, M. Valentini, D. Topwal, D. D. Sarma, S. Lupi, and P. Postorino, Phys. Rev. B **84**, 235134 (2011).
[10] S. S. Streltsov, A. O. Shorikov, S. L. Skornyakov, A. I. Poteryaev, and D. I. Khomskii, Sci. Rep. **7**, 13005 (2017).
[11] J. Guo, Y. Qi, S. Matsuishi, and H. Hosono, J. Am. Chem. Soc. **134**, 20001 (2012).
[12] Y. Qi, S. Matsuishi, J. Guo, H. Mizoguchi, and H. Hosono, Phys. Rev. Lett. **109**, 217002 (2012).
[13] J. Guo, Y. Qi, and H. Hosono, Phys. Rev. B **87**, 224504 (2013).
[14] M. A. ElGhazali, P. G. Naumov, H. Mirhosseini, V. Süß, L. Müchler, W. Schnelle, C. Felser, and S. A. Medvedev, Phys. Rev. B **96**, 060509(R) (2017).
[15] C. Soulard, X. Rocquefelte, P. E. Petit, M. Evain, S. Jobic, J. P. Itié, P. Munsch, H. J. Koo, and M. H. Whangbo, Inorg. Chem. **43**, 1943 (2004).
[16] I. B. Bersuker, Chem. Rev. **113**, 1351 (2013).
[17] I. Bersuker, *The Jahn-Teller Effect* (Cambridge University Press, Cambridge, 2006).
[18] A. D. Oyedele, S. Yang, L. Liang, A. A. Puretzky, K. Wang, J. Zhang, P. Yu, P. R. Pudasaini, A. W. Ghosh, Z. Liu, C. M. Rouleau, B. G. Sumpter, M. F. Chisholm, W. Zhou, P. D. Rack, D. B. Geohegan, and K. Xiao, J. Am. Chem. Soc. **139**, 14090 (2017).
[19] K. I. Kugel and D. I. Khomskiĭ, Sov. Phys. Usp. **25**, 231 (1982).

[20] J. S. Schilling, in *Handbook of High-Temperature Superconductivity: Theory and Experiment*, edited by J. R. Schrieffer and J. S. Brooks (Springer, New York, 2007), p. 427.
[21] J. A. Wilson, Adv. Phys. **21**, 143 (1972).
[22] J. M. Honig and J. Spałek, Chem. Mater. **10**, 2910 (1998).
[23] C. d. l. Heras and F. Agulló-Rueda, J. Phys.: Condens. Matter **12**, 5317 (2000).
[24] A. K. Kleppe and A. P. Jephcoat, Mineral. Mag. **68**, 433 (2004).
[25] P. G. Naumov, M. A. ElGhazali, and S. A. Medvedev (unpublished).